THE JOURNAL OF PHYSICAL CHEMISTRY Letters

Letter

pubs.acs.org/JPCL

Imaging Excited-State Dynamics of Doped He Nanodroplets in Real-Time

Johannes von Vangerow,[†] François Coppens,[‡] Antonio Leal,[§] Martí Pi,[§] Manuel Barranco,[§,‡] Nadine Halberstadt,[‡] Frank Stienkemeier,[†] and Marcel Mudrich*[,†]

[†]Physikalisches Institut, Universität Freiburg, Hermann-Herder-Str. 3, 79104 Freiburg, Germany

[‡]Laboratoire des Collisions, Agrégats, Réactivité, IRSAMC, UMR 5589, CNRS et Université Paul Sabatier-Toulouse 3, 118 route de Narbonne, F-31062 Toulouse Cedex 09, France

[§]Departament FQA, Facultat de Física, and IN2UB, Universitat de Barcelona, Diagonal 645, 08028 Barcelona, Spain

Supporting Information

ABSTRACT: The real-time dynamics of excited alkali metal atoms (Rb) attached to quantum fluid He nanodroplets is investigated using femtosecond imaging spectroscopy and time-dependent density functional theory. We disentangle the competing dynamics of desorption of excited Rb atoms off the He droplet surface and solvation inside the droplet interior as the Rb atom is ionized. For Rb excited to the 5p and 6p states, desorption occurs on starkly differing time scales (∼100 versus ∼1 ps, respectively). The comparison between theory and experiment indicates that desorption proceeds either impulsively (6p) or in a transition regime between impulsive dissociation and complex desorption (5p).

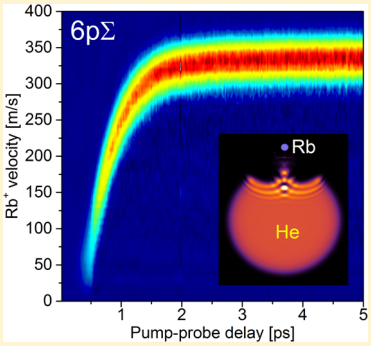

He nanodroplets are intriguing quantum fluid objects of finite size capable of efficiently capturing and cooling atoms, molecules, and clusters for spectroscopy and dynamics studies.[1,2] Upon electronic excitation, embedded atoms and small molecules tend to move toward the droplet surface and may be ejected due to short-range electron He repulsion.[3] In contrast, cations experience attractive forces toward the He droplets mediated by electrostatic polarization, which draw them to the droplet interior, where they may form snowball complexes.[4−7] These two opposing trends lead to a rich dynamics initiated by photoexcitation of embedded species involving desorption, electronic relaxation, complex formation, as well as solvation and desolvation of the ionized impurity.[8−19] Similar dynamics have been observed when exciting pure He droplets with extreme-ultraviolet radiation[20] as well as for other types of clusters.[21]

So far, time-resolved experiments on He droplets doped with alkali (Ak) metal atoms were mostly focused on the formation of AkHe exciplexes induced by laser excitation.[15−18,22,23] The concurrent desorption of these excited species was estimated to proceed on a picosecond time scale.[9,10,13,24−26] This estimate, sufficient for studies employing nanosecond laser pulses, clearly lacks precision for experiments with sub-picosecond time resolution. Thus in the previous measurements as well as in experiments focusing on electronic and vibrational coherences of Ak atoms and molecules[17,19,22,23,27] the exact location of the dopants, attached to the droplets or in the vacuum, has remained somewhat uncertain.

Here we report a combined experimental and theoretical investigation of the excited-state dynamics of doped He nanodroplets in real time. The combination of fs pump−probe spectroscopy with velocity map imaging (VMI)[28] allows us to clearly disentangle complex formation, desorption, and ion solvation. As a model system, we investigate He droplets doped with single rubidium (Rb) atoms. Ground-state Rb atoms and small molecules are weakly bound to the He droplet surface in a dimple structure.[29−31] Therefore, the ejection dynamics of the excited Rb atom (Rb*) is not affected by processes such as the interaction of Rb* with density waves traveling in the bulk of the droplet, as for Ag*.[11]

We excite droplet-bound Rb atoms to states correlating either to the lowest excited state 5p or to the higher lying state 6p. The dynamics is probed by ionizing Rb* at variable delay times between photoexcitation ($t = 0$) and photoionization ($t = t_+$) while monitoring the velocity and signal yield of Rb^+ ions. A simulation based on time-dependent density functional theory (TDDFT) gives us insight into the time evolution both of Rb* and of the Rb^+ ion taking into account the quantum fluid properties of the He environment. Using these techniques, we follow the trajectory of the excited and subsequently ionized Rb atom in detail as it escapes from the droplet surface or submerges into it. Although separated by only ∼1.4 eV in energy, the two states 5p and 6p are found to feature time

Received: November 6, 2016
Accepted: December 20, 2016
Published: December 20, 2016

DOI: 10.1021/acs.jpclett.6b02598
J. Phys. Chem. Lett. 2017, 8, 307−312

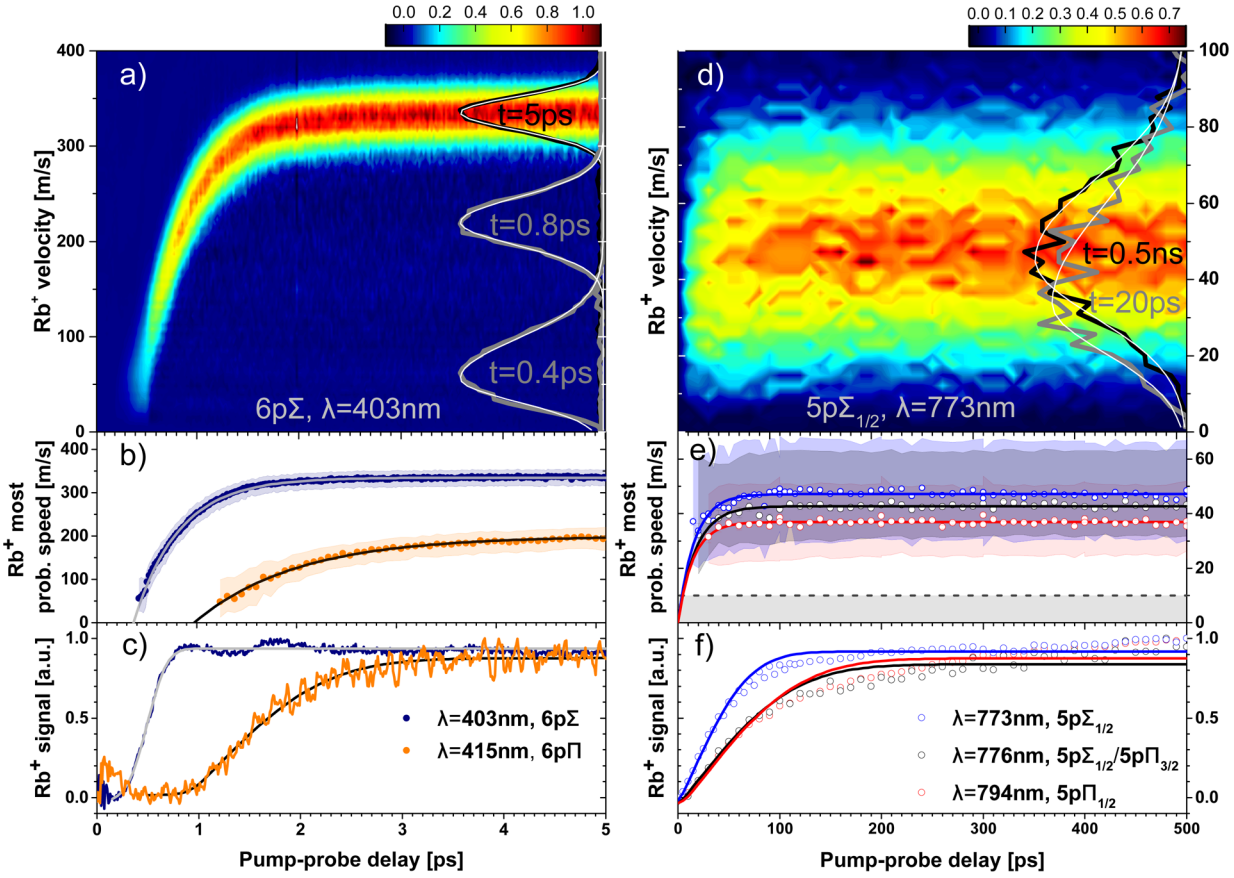

Figure 1. Rb^+ transient speed distributions (a,d), most probable speeds (b,e), and ion yields (c,f) resulting from photoexcitation to He droplet perturbed states correlating to 6p (left column) and 5p states (right column) of Rb (pump) and subsequent ionization (probe). The shaded areas (b,e) indicate the left and right $e^{-1/2}$ widths of the speed distributions. The shaded area at the bottom of panel e depicts the experimental resolution. The smooth lines are fits to the data (see text).

constants of the desorption dynamics differing by about 2 orders of magnitude.

Figure 1a,d shows examples of measured Rb^+ transient speed distributions derived from the VMIs by angular integration. From these distributions we infer the most probable speeds (b,e) by fitting a skewed Gaussian distribution as illustrated by selected speed distributions shown on the right-hand sides of Figure 1a,d.[34] For the droplet perturbed Rb 6p states the most probable speeds (b) as well as the total Rb^+ ion yields (c) show a steep rise within a few picoseconds. In contrast, for the droplet perturbed 5p states we record speed distributions (e) close to our experimental resolution of ~10 m/s (shaded gray area) and ion yields (f) which increase within hundreds of picoseconds.

For the droplet perturbed Rb 6p excitations, the transient ion yield curves (c) have previously been interpreted in terms of the competing effects of repulsion from the He droplet surface and attraction of Rb^+ toward it.[14] Accordingly, the slower dynamics of the 6pΠ state compared with that of the 6pΣ state is due to the weaker repulsion from the droplet. We term "fall-back time", τ_c, the critical delay discriminating between the ion falling back into the droplet and the ion escaping into the vacuum. It is obtained by fitting the 6p and 5p ion yield data with a piecewisely defined asymmetric error function $I(t) = A_0 + A\cdot\{[t \le \mu]\sigma_-\cdot\mathrm{erf}[(t-\mu)/\sigma_-] + [t > \mu]\,\sigma_+\cdot\mathrm{erf}[(t-\mu)/\sigma_+]\}$, where $\sigma_{\mp}$ denote widths on the right and left side of the inflection point μ. τ_c is obtained from computing the 50% rise time of that fit function. The evolution of the most probable speeds $\hat{v}$ is fitted by $\hat{v}(t) = \hat{v}_f\{1-\exp[-\ln 2\cdot(t-t_0)/\tau]\}$, from which we obtain the characteristic 50% rise times $\tau_v = t_0 + \tau$.

Note that for each applied pump−probe delay we measure the final velocity distribution of the ion after it has fully escaped from the droplet. Therefore, the experiment does not give direct access to the desorption dynamics of the neutral Rb* atom. To get a complete picture of the dynamics, simulations based on the TDDFT approach are carried out using the functional of ref 35. Details of this approach have been described before.[9,11,32] In short, we consider droplets consisting of $N = 1000$ atoms doped with one Rb atom. Because of its large mass compared with that of He we describe the dynamics of the Rb atom classically. The simulations of the full pump−probe sequence consist of two steps: the propagation of Rb* in the excited state starting at $t = 0$ (step 1) and the propagation of the Rb^+ ion at times $t > t_+$ (step 2). This is achieved by solving the coupled 3D TDDFT and Newton's equations for the He droplet and the Rb impurity, respectively.

In step 1, the Rb*−droplet interaction is obtained from the Rb*−He $n\Sigma$ and $n\Pi$ pair potentials[36] with $n = 5$ and 6, and includes the spin−orbit interaction in the usual He−Rb* distance-independent way; it also allows for the dynamic evolution of the internal electronic state of the Rb* atom.[11] In step 2, the coupled dynamical equations are now simpler as they do not explicitly take into account the electronic structure of the closed-shell Rb^+ ion. In all simulations, a spatial grid of 0.4 Å and a time step of 0.5 fs are used.

DOI: 10.1021/acs.jpclett.6b02598
J. Phys. Chem. Lett. 2017, 8, 307−312

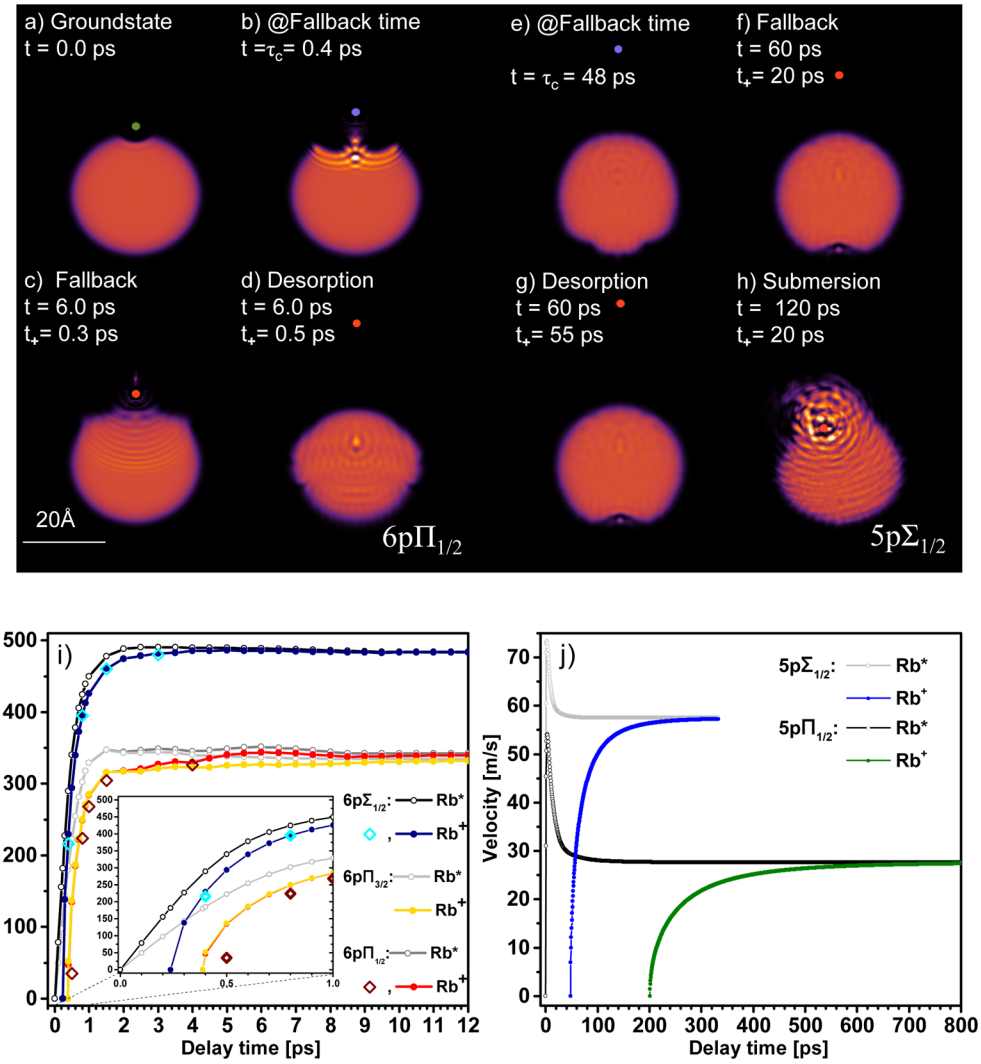

Figure 2. TDDFT-based 2D densities (a–d,e–h) and velocities (i,j) of Rb atoms attached to He_{1000} excited from equilibrium (a) to droplet perturbed 6p (left column) and 5p (right column) states. Configurations are shown for different propagation times t and ionization times t_+: (b,e) neutral Rb at fall-back time $t = \tau_c$; (c,f) $t_+ < \tau_c$, fall-back of Rb^+ ion; (d,g) $t_+ > \tau_c$, desorption of Rb^+; (h) solvation of Rb^+; (i,j) evolution of Rb* velocities with time t (gray open dots), and final velocities of Rb^+ (colored filled dots) as a function of t_+.

For step 1, initial conditions are given by the structure of the neutral Rb–He_{1000} complex in the ground state[32] obtained using the Rb–He potential of ref 37. For step 2 the initial conditions are given by the step 1 simulation at $t = t_+$. Carrying out the full simulations for step 2 is crucial for short and intermediate delays $t_+ \lesssim \tau_c$, as the droplet is still far from being relaxed when Rb* is photoionized. At variance, we have checked that keeping the droplet density frozen as done in ref 14 is a good approximation for long delays $t_+ \gg \tau_c$. In Figure 2i the open diamonds show the difference between carrying out the full simulation and keeping the He density frozen at $t = \tau_c$ for $t_+ \gtrsim \tau_c$ (filled dots). For illustration, these simulations are provided as animations in the Supporting Information.

Figure 2a–d,e–h shows snapshots of the resulting 2D densities for different propagation times t and ionization times t_+ for the $6p\Pi_{1/2}$ (left column) and $5p\Sigma_{1/2}$ (right column) states. The ground-state dimple configuration is depicted in panel a. Figure 2b,e shows the configurations at the fall-back time τ_c. Panels c, d and g, h illustrate the desorption and fall-back processes. When ionization occurs before the fall-back time, $t_+ < \tau_c$, the ion turns around and submerges into the droplet, where it becomes fully solvated (h). For $t_+ > \tau_c$, the ion keeps moving away from the droplet surface and fully desorbs (d, g). Panels i, j show the velocities of Rb* (open symbols) and Rb^+ ions (filled symbols). The inset shows a close-up of the 6p dynamics at short propagation times.

For the 6p states, the Rb* velocity features a steep rise that levels out after ~2 ps propagation time t (gray open dots). The final Rb^+ velocity is reduced compared with the Rb* velocity at short delays $t_+ \lesssim 10$ ps (colored dots) due to the attraction of the Rb^+ ion toward the He droplet. For long delays these values converge as the Rb^+–He droplet attraction drops off at large distances. For the 5p case, the Rb* velocity shows an overshoot at short delays relative to the asymptotic value. This is due to the transient Rb*–He droplet interaction being weakly attractive at intermediate distance, which slows down the ejected Rb* atom. It derives from the Rb*–He potentials featuring an outer attractive region.

A compilation of the time constants for fall-back, τ_c, rise times of the ion speed, τ_v, as well as most probable Rb^+ final velocities, $\hat{v}_f$, inferred from the experimental and theoretical data, is presented in Figure 3. The theory values of τ_v are

DOI: 10.1021/acs.jpclett.6b02598
J. Phys. Chem. Lett. 2017, 8, 307–312

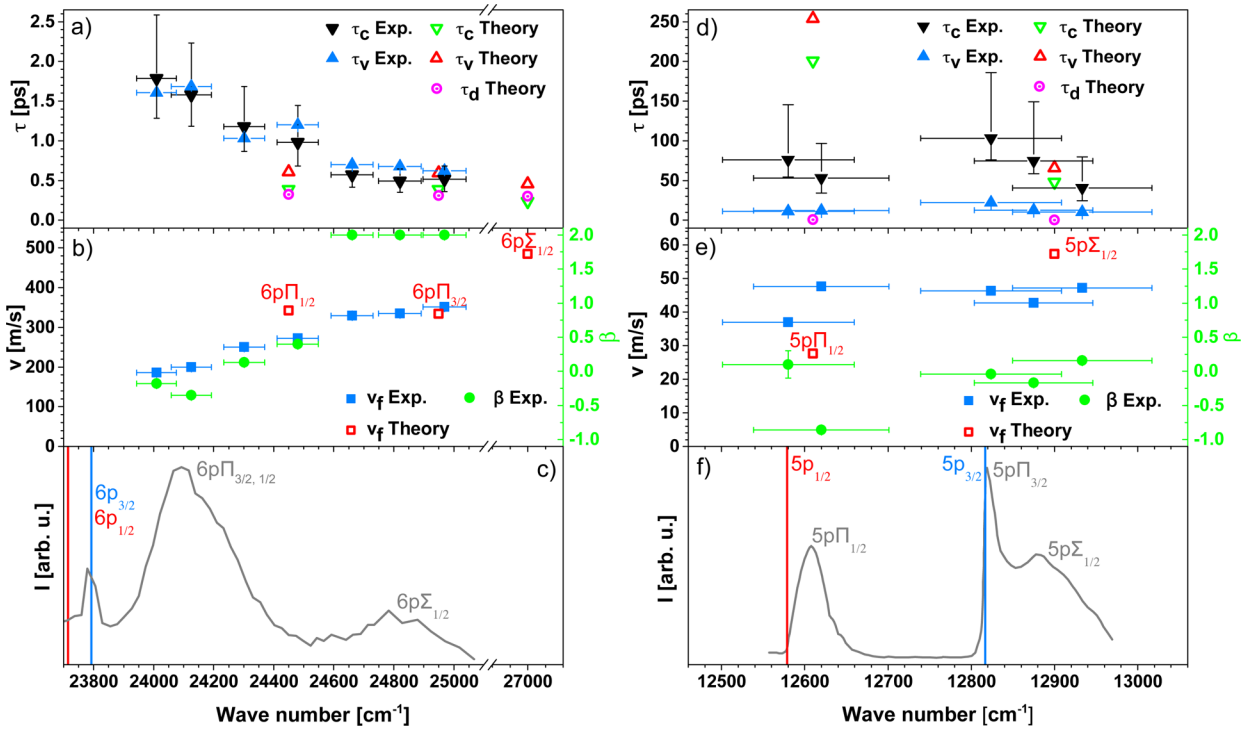

Figure 3. Experimental and theoretical fall-back time constants τ_c (a,d), velocity rise times τ_v (a,d), theoretical Rb* desorption times τ_d (a,d), Rb^+ final most probable speeds $\hat{v}_f$ (b,e), and anisotropy parameters β (b,e) for different excitation wavenumbers corresponding to droplet perturbed Rb states 6p (left column) and 5p (right column). Panels c and f show fluorescence emission spectra as reference.[25,38] Vertical lines indicate free atomic transitions.

determined by fitting the final ion velocities using the same model as for the experimental data. In addition, Figure 3a,d contains desorption times τ_d of the neutral Rb* atoms inferred from the simulation by fitting the same model as for ion velocities. Note that for the $5p\Pi_{1/2}$ and $5p\Sigma_{1/2}$ states we obtain values τ_d = 0.4 and 0.2 ps, respectively, from the rising edges of the speed curves in Figure 2j. Figure 3b,e displays the anisotropy parameter β of the Rb^+ angular distributions measured at long delay times. For reference we include the corresponding fluorescence excitation spectra taken from literature.[25,38] Excitation wavenumbers for the theory values correspond to the peak positions of the simulated absorption spectra (not shown). Vertical error bars are connected to widths of the asymmetric fit function. Horizontal error bars reflect the spectral widths (FWHM) of the fs laser pulses.

The experimentally observed drastic difference between time scales for the 6p and 5p state dynamics is well-reproduced by the calculation. The general trend that fall-back times τ_c decrease and final velocities rise as a function of excitation wavenumber reflects the increasing repulsion acting between Rb* and the He droplet as the excitation energy is tuned up.[9,13,24,26,32] Fall-back times τ_c and speed rise times τ_v exceed the desorption times τ_d of the neutral Rb* atom because the range of Rb^+–He attractive interaction is larger than that of Rb*–He repulsion.[14]

Discrepancies are found for the asymptotic velocities of the 6p states that are smaller in the experiment than in the simulation by a factor of ~0.7. Accordingly, experimental fall-back and speed rise times exceed the simulated values by a factor of 2 for the $6p\Sigma_{1/2}$ and up to a factor of 4 for the 6pΠ states. We attribute this mainly to the limited accuracy of the 6pΣ and 6pΠ Rb*-He pair potentials[36] used in the simulation, causing a substantial blue shift of the simulated 6p ← 5s absorption spectrum (not shown) with respect to the measured one.[24,25]

For the 5p states the fall-back times being considerably larger than the speed rise times indicates that the desorption dynamics deviates to some extent from the impulsive model. In the limit of statistical desorption of Rb* atoms by an evaporation-like process, one would expect a continuously rising yield of free atoms and broad thermal distributions. Considering the slightly delayed, slow rise of the Rb^+ yield (Figure 1f) and the peaked but broadened speed distributions that feature only small up-shifts at short delays (Figures 1d,e), we conclude that the dynamics of 5p excited states proceeds in a transition regime from impulsive dissociation to more complex, evaporation-like desorption. This conclusion is supported by the anisotropy parameter β (Figure 3e), whose sign correctly indicates the symmetry of the dissociating complex[9,13,24] but whose absolute value is significantly reduced compared with that expected for impulsively dissociating complexes, in contrast with the 6p case (Figure 3b). Consequently, the quantitative agreement with the simulations, which do describe complex dynamical couplings within the superfluid model (Figure 2j) but do not contain statistical evaporation, is limited.

Aside from this, the experimentally observed higher final ion velocity and smaller fall-back time for the $5p\Pi_{1/2}$ state compared with theory may be due to the measured signals being dominated by excitation of the blue edge of the $5p\Pi_{1/2}$ feature. Considering the observed steep rise of fall-back time and drop of Rb^+ velocity toward the red edge of the $5p\Pi_{1/2}$ feature, our results agree with the previous finding that Rb* remains attached to the droplet surface upon narrow-band excitation at the red edge of the $5p\Pi_{1/2}$ state.[39,40]

DOI: 10.1021/acs.jpclett.6b02598
J. Phys. Chem. Lett. 2017, 8, 307–312

Excitation of the $5p\Pi_{3/2}$ state leads to the formation of RbHe exciplexes because the Rb*He pair interaction is strongly attractive in this state.[15,16,38] While exciplex formation is reproduced by the simulation, the ejection of exciplexes off the He droplet surface is not. However, we find that nonradiative relaxation to the $5p\Pi_{1/2}$ state may supply enough kinetic energy to the Rb* atom to cause ejection. We therefore argue that when tuning the fs laser to the $5p\Pi_{3/2}$ peak, the experimentally observed Rb^+ signal is mainly due to spin relaxation to the $5p\Pi_{1/2}$ state.[38] Possibly the admixture of the nearby repulsive $5p\Sigma_{1/2}$ state also contributes. The relaxation dynamics will be further studied using time-resolved photoelectron spectroscopy. Let us mention that the $RbHe^+$ pump−probe transients (not shown) closely follow the ones of Rb^+ but significantly differ from those previously measured using a one-color NIR scheme.[15,22] This raises some doubts as to the previous interpretation in terms of exciplex formation times and should be further investigated.

In conclusion, the observed dynamics of femtosecond pump−probe photoionization of Rb atoms attached to He nanodroplets is determined by the competition between the repulsive interaction of the droplet with the Rb atom in an excited state and the attractive interaction of the droplet with the Rb^+ cation, causing either desorption of Rb* off the droplet or submersion of the Rb^+ ion into the droplet interior, respectively. The resulting desorption dynamics proceeds impulsively within ∼1 ps for the 6p excited states and in a transition regime between impulsive dissociation and statistical desorption within ∼100 ps for the 5p states. This interplay between opposing trends (Rb* repulsion, Rb^+ attraction) is likely to be present in other types of clusters and condensed phase systems probed by time-resolved photoionization spectroscopy.

EXPERIMENTAL METHODS

The experimental setup has been previously described.[14,32] In brief, He droplets with an average diameter of 10 nm are created by continuous supersonic expansion and doped by one Rb atom on average.[14,32] The laser system generates amplified pulses of 100 fs duration at a repetition rate of 5 kHz with a tunable center wavelength in the near-infrared (NIR) region. Light in the visible range (VIS) is generated by frequency doubling. Pulses are split and separated in time in a Mach−Zehnder type interferometer. Droplet perturbed Rb 6p and 5p states are probed by one-color VIS and two-color NIR+VIS pump−probe schemes, respectively. NIR pulses are strongly attenuated to avoid excitations to higher lying states. Photoions are detected by a VMI spectrometer.[24,28,32] For varying pump−probe delay steps, mass-selected ion VMIs are recorded and inverse-Abel transformed.[33] For each pump−probe scheme, a background contribution from ionization of effusive Rb is observed. In the measurement probing the Rb 6p states, additional background arises from single pulse ionization. To extract the pump−probe correlated dynamics, these contributions are subtracted from the signal.

ASSOCIATED CONTENT

Supporting Information

The following files are available free of charge. The Supporting Information is available free of charge on the ACS Publications website at DOI: 10.1021/acs.jpclett.6b02598.

Desorption and fall-back dynamics of Rb atoms initially excited to the $5p\Pi_{1/2}$ state and ionized at t_+ = 20 ps. (AVI)

Desorption dynamics for $5p\Pi_{1/2}$ excitation and t_+ = 55 ps. (AVI)

Desorption and fall-back dynamics for $6p\Pi_{1/2}$ excitation t_+ = 0.3 ps. (AVI)

Desorption dynamics for $6p\Pi_{1/2}$ excitation and t_+ = 0.5 ps. (AVI)

AUTHOR INFORMATION

Corresponding Author

*E-mail: mudrich@physik.uni-freiburg.de.

ORCID

Marcel Mudrich: 0000-0003-4959-5220

Notes

The authors declare no competing financial interest.

ACKNOWLEDGMENTS

Financial support for this work by the Deutsche Forschungsgemeinschaft (grant nos. MU 2347/6-1 and IRTG 2079), DGI, Spain (grant no. FIS2014-52285-C2-1-P), and HPC resources from CALMIP (Grant P1039) is gratefully acknowledged. M.B. thanks the Université Fédérale Toulouse Midi-Pyrénées for financial support through the "Chaires d'Attractivité 2014" program IMDYNHE.

REFERENCES

(1) Toennies, J. P.; Vilesov, A. F. *Angew. Chem., Int. Ed.* **2004**, *43*, 2622.

(2) Stienkemeier, F.; Lehmann, K. *J. Phys. B: At., Mol. Opt. Phys.* **2006**, *39*, R127.

(3) Brauer, N. B.; Smolarek, S.; Loginov, E.; Mateo, D.; Hernando, A.; Pi, M.; Barranco, M.; Buma, W. J.; Drabbels, M. *Phys. Rev. Lett.* **2013**, *111*, 153002.

(4) Tiggesbäumker, J.; Stienkemeier, F. *Phys. Chem. Chem. Phys.* **2007**, *9*, 4748−4770.

(5) Müller, S.; Mudrich, M.; Stienkemeier, F. *J. Chem. Phys.* **2009**, *131*, 044319.

(6) Theisen, M.; Lackner, F.; Ernst, W. E. *Phys. Chem. Chem. Phys.* **2010**, *12*, 14861−14863.

(7) Zhang, X.; Drabbels, M. *J. Chem. Phys.* **2012**, *137*, 051102.

(8) Smolarek, S.; Brauer, N. B.; Buma, W. J.; Drabbels, M. *J. Am. Chem. Soc.* **2010**, *132*, 14086−14091.

(9) Hernando, A.; Barranco, M.; Pi, M.; Loginov, E.; Langlet, M.; Drabbels, M. *Phys. Chem. Chem. Phys.* **2012**, *14*, 3996−4010.

(10) Loginov, E.; Drabbels, M. *J. Chem. Phys.* **2012**, *136*, 154302.

(11) Mateo, D.; Hernando, A.; Barranco, M.; Loginov, E.; Drabbels, M.; Pi, M. *Phys. Chem. Chem. Phys.* **2013**, *15*, 18388−18400.

(12) Leal, A.; Mateo, D.; Hernando, A.; Pi, M.; Barranco, M.; Ponti, A.; Cargnoni, F.; Drabbels, M. *Phys. Rev. B: Condens. Matter Mater. Phys.* **2014**, *90*, 224518.

(13) Loginov, E.; Hernando, A.; Beswick, J. A.; Halberstadt, N.; Drabbels, M. *J. Phys. Chem. A* **2015**, *119*, 6033−6044.

(14) von Vangerow, J.; John, O.; Stienkemeier, F.; Mudrich, M. *J. Chem. Phys.* **2015**, *143*, 034302.

(15) Droppelmann, G.; Bünermann, O.; Schulz, C. P.; Stienkemeier, F. *Phys. Rev. Lett.* **2004**, *93*, 0233402.

(16) Reho, J.; Higgins, J.; Lehmann, K. K.; Scoles, G. *J. Chem. Phys.* **2000**, *113*, 9694−9701.

(17) Mudrich, M.; Droppelmann, G.; Claas, P.; Schulz, C.; Stienkemeier, F. *Phys. Rev. Lett.* **2008**, *100*, 023401.

(18) Mudrich, M.; Stienkemeier, F. *Int. Rev. Phys. Chem.* **2014**, *33*, 301−339.

DOI: 10.1021/acs.jpclett.6b02598
J. Phys. Chem. Lett. 2017, 8, 307−312

(19) Bruder, L.; Mudrich, M.; Stienkemeier, F. *Phys. Chem. Chem. Phys.* **2015**, *17*, 23877−23885.
(20) Ziemkiewicz, M. P.; Neumark, D. M.; Gessner, O. *Int. Rev. Phys. Chem.* **2015**, *34*, 239.
(21) Masson, A.; Poisson, L.; Gaveau, M.-A.; Soep, B.; Mestdagh, J.-M.; Mazet, V.; Spiegelman, F. *J. Chem. Phys.* **2010**, *133*, 054307.
(22) Schulz, C. P.; Claas, P.; Stienkemeier, F. *Phys. Rev. Lett.* **2001**, *87*, 153401.
(23) Giese, C.; Mullins, T.; Grüner, B.; Weidemüller, M.; Stienkemeier, F.; Mudrich, M. *J. Chem. Phys.* **2012**, *137*, 244307.
(24) Fechner, L.; Grüner, B.; Sieg, A.; Callegari, C.; Ancilotto, F.; Stienkemeier, F.; Mudrich, M. *Phys. Chem. Chem. Phys.* **2012**, *14*, 3843.
(25) Pifrader, A.; Allard, O.; Auböck, G.; Callegari, C.; Ernst, W.; Huber, R.; Ancilotto, F. *J. Chem. Phys.* **2010**, *133*, 164502.
(26) Loginov, E.; Drabbels, M. *J. Phys. Chem. A* **2014**, *118*, 2738−2748.
(27) Grüner, B.; Schlesinger, M.; Heister, P.; Strunz, W. T.; Stienkemeier, F.; Mudrich, M. *Phys. Chem. Chem. Phys.* **2011**, *13*, 6816−6826.
(28) Eppink, A. T. J. B.; Parker, D. H. *Rev. Sci. Instrum.* **1997**, *68*, 3477.
(29) Ancilotto, F.; DeToffol, G.; Toigo, F. *Phys. Rev. B: Condens. Matter Mater. Phys.* **1995**, *52*, 16125−16129.
(30) Stienkemeier, F.; Higgins, J.; Ernst, W. E.; Scoles, G. *Phys. Rev. Lett.* **1995**, *74*, 3592−3595.
(31) Bünermann, O.; Droppelmann, G.; Hernando, A.; Mayol, R.; Stienkemeier, F. *J. Phys. Chem. A* **2007**, *111*, 12684.
(32) von Vangerow, J.; Sieg, A.; Stienkemeier, F.; Mudrich, M.; Leal, A.; Mateo, D.; Hernando, A.; Barranco, M.; Pi, M. *J. Phys. Chem. A* **2014**, *118*, 6604−6614.
(33) Dick, B. *Phys. Chem. Chem. Phys.* **2014**, *16*, 570−580.
(34) Mudholkar, G. S.; Hutson, A. D. *J. Stat. Plan. Inference* **2000**, *83*, 291−309.
(35) Ancilotto, F.; Barranco, M.; Caupin, F.; Mayol, R.; Pi, M. *Phys. Rev. B: Condens. Matter Mater. Phys.* **2005**, *72*, 214522.
(36) Pascale, J. *Phys. Rev. A: At., Mol., Opt. Phys.* **1983**, *28*, 632−644.
(37) Patil, S. H. *J. Chem. Phys.* **1991**, *94*, 8089−8095.
(38) Brühl, F. R.; Trasca, R. A.; Ernst, W. E. *J. Chem. Phys.* **2001**, *115*, 10220−10224.
(39) Auböck, G.; Nagl, J.; Callegari, C.; Ernst, W. E. *Phys. Rev. Lett.* **2008**, *101*, 035301.
(40) Theisen, M.; Lackner, F.; Ernst, W. E. *J. Phys. Chem. A* **2011**, *115*, 7005−7009.

DOI: 10.1021/acs.jpclett.6b02598
J. Phys. Chem. Lett. 2017, 8, 307−312